3-1-2007

Integration of hydrogels with hard and soft microstructures

Ming Li
University of Minnesota

Babak Ziaie
Birck Nanotechnology Center, Purdue University, bziaie@purdue.edu

Eric Nuxoll
University of Minnesota

Kristóf Iván
Budapest University of Technology and Economics

Ronald A. Siegel
University of Minnesota

Journal of
Nanoscience and Nanotechnology
Vol. 7, 780–789, 2007

Integration of Hydrogels with Hard and Soft Microstructures

Ming Lei[1], Babak Ziaie[2], Eric Nuxoll[3], Kristóf Iván[4], Zoltán Noszticzius[4], and Ronald A. Siegel,[3,5,*]

[1] *Department of Electrical and Computer Engineering, University of Minnesota, Minneapolis, MN 55455, USA*
[2] *School of Electrical and Computer Engineering, Purdue University, West Lafayette, IN 47907, USA*
[3] *Department of Pharmaceutics, University of Minnesota, Minneapolis, MN 55455, USA*
[4] *Center for Complex and Nonlinear Systems and the Department of Chemical Physics, Budapest University of Technology and Economics, H-1521 Budapest, Hungary*
[5] *Department of Biomedical Engineering, University of Minnesota, Minneapolis, MN 55455, USA*

Hydrogels, i.e., water-swollen polymer networks, have been studied and utilized for decades. These materials can either passively support mass transport, or can actively respond in their swelling properties, enabling modulation of mass and fluid transport, and chemomechanical actuation. Response rates increase with decreasing hydrogel dimension. In this paper, we present three examples where incorporation of hydrogels into solid microstructures permits acceleration of their response, and also provides novel functional capabilities. In the first example, a hydrogel is immobilized inside microfabricated pores within a thin silicon membrane. This hydrogel does not have a swelling response under the conditions investigated, but under proper conditions it can be utilized as a part of an electrolytic diode. In the second example, hydrogels are polymerized under microcantilever beams, and their swelling response to pH or glucose concentration causes variable deflection of the beam, observable under a microscope. In the third example, swelling and shrinking of a hydrogel embedded in a microfabricated valve structure leads to chemical gating of fluid motion through that valve. In all cases, the small size of the system enhances its response rate.

Keywords: Hydrogels, Micromechanics, Microfluidics, Electrolyte Diode, Microcantilever, Microvalve, Microsensing, Drug Delivery.

1. INTRODUCTION

Hydrogels are crosslinked polymer networks that absorb water, or swell. These materials display properties characteristic of both solids and liquids. Like solids, hydrogels recover their initial shape following release from deformation. Like liquids, however, hydrogels can support fluid convection and diffusion of solutes that are small enough to fit within the mesh defined by the polymer and crosslinks. Biological connective tissues such as cartilage, corneal stroma, and basement membrane are essentially hydrogels consisting of the fibrous protein collagen, and proteoglycans.[1–3] Synthetic hydrogels have found utility as soft contact lenses,[4,5] ion exchangers,[6,7] stationary chromatography phases,[8] substrates for enzyme immobilization,[9] and as components of drug delivery systems.[10]

A remarkable property of certain hydrogels is their responsiveness to changes in the external environment. Depending on a hydrogel's structure and chemical composition, its dimensions can change in response to alterations in environmental temperature,[11–13] pH,[14–19] ionic strength,[20,21] electric field,[22,23] magnetic field,[24] light,[25,26] or concentration of specific analytes.[27–30] When mechanically constrained, responsive hydrogels exert swelling forces on the constraining structures. A hydrogel's response may be continuous or discrete, depending on the nature of the hydrogel and the applied stimulus.[31] It has been shown that discrete changes in hydrogel swelling are first order phase transitions, analogous to gas–liquid transitions.[32]

The responsiveness of hydrogels to environmental stimuli has motivated research into their applications as components of sensors and actuators, including artificial muscles,[33,34] pH-, temperature- and glucose sensors,[28,35] environmentally-triggered drug delivery devices,[16,36–43] and flow-control valves. Utilization of stimuli-responsive hydrogels in separation processes has also been explored.[8,44,45] Realization of many of these applications has been stalled, however, due to mechanical weakness of

*Author to whom correspondence should be addressed.

 1533-4880/2007/7/780/010 doi:10.1166/jnn.2007.513

hydrogels, and sluggishness of response. Furthermore, just as an isolated muscle can contract but perform little useful work unless it is attached to a solid bony structure, it may be difficult to exploit the thermo- or chemomechanical responsiveness of a hydrogel unless it is integrated into or onto a solid framework.

The mechanical weakness problem is attributed primarily to heterogeneity of crosslinked network structure, leading to rapid formation and propagation of breakages.[46] Three solutions to this problem have been proposed recently:

(1) inclusion of a second network that dissipates stress produced at breakage points;[47]

(2) deleting tetrafunctional divinyl crosslinkers from the pregel solution and including exfoliated clay nanoplates, which adsorb the polymerization initiator and therefore become polyfunctional crosslink sites;[48] and

(3) synthesizing hydrogels with sliding, rotaxane-based crosslinks.[49]

These techniques have been explored with particular systems, and much work remains to determine whether they can be generalized and applied routinely.

Swelling and deswelling dynamics of a hydrogel are governed by osmotic, elastic, and viscous stresses that arise when the external environment is altered. It has been shown that these dynamics are governed by a diffusion-like equation, where the "diffusivity" is related to the elastic modulus of the polymer network and its fluid (Darcy) permeability.[50–52] Consequently, characteristic times for hydrogel swelling and deswelling scale as the square of the smallest gel dimension. The same scaling relation applies for diffusion of solutes through or out of a hydrogel, although here the relevant diffusivity corresponds to restricted Brownian motion of solute inside the hydrated polymer network.[53–57] Thus, while millimeter-sized hydrogels respond on time scales of hours or days to changes in external environment, micron- or submicron-sized hydrogels respond nearly instantaneously, or within seconds. Unfortunately, size-reduction also reduces loading capacity of individual hydrogels for releasable solutes, which may be a disadvantage when multiple cycles of solute release and retention are desired. (This latter problem may be obviated by incorporation of micro- or nanogels into a matrix, however.)[58, 59]

In this paper, we present three examples in which micron-scale hydrogels are integrated into solid or elastic microstructures, leading to rapid response and novel function. In the first example, a microgel spans a thin, solid membrane structure, and serves as a medium supporting ion migration when an electric field is imposed. Under proper conditions, a rectified, diode-like current–voltage characteristic is achieved. In the second example, expansion and contraction of a microgel in response to chemical stimuli causes distortion of a microcantilever beam. In the third example, similar chemomechanical response of a microgel is used to open and shut a microfluidic valve.

2. MICROELECTROCHEMICAL RECTIFIER

While electrons and holes carry currents in metals and semiconductors, conduction in aqueous solutions is due to drift of cations from anode to cathode, and anions in the opposite direction. The conductance of an electrolyte solution is proportional to the concentrations and electrical mobilities of the constituent ions.

When a neutrally charged hydrogel, swollen in pure water, is interposed between two well-stirred salt solutions of equal concentration, and a voltage is imposed between the two solutions, with electrodes close to the hydrogel surfaces, the resistance will be high initially, since the only ions in the hydrogel that can drift are H^+ and OH^- formed by dissociation of water. Over time, however, salt ions diffuse into the hydrogel, lowering resistance and permitting current to flow. In addition to diffusion, the electric field drives cations into the gel from the anodic side, and anions from the cathodic side. The final current–voltage characteristic is expected to be linear in this case, with conductance increasing with salt concentration. For a hydrogel of given composition and structure, the characteristic time for equilibration of salt in the hydrogel, and establishment of final current value, is proportional to the square of the hydrogel thickness.

Suppose now that the hydrogel is exposed on one side to a basic aqueous solution. BOH, which dissociates into OH^- and a cation B^+, while the other side is exposed to an aqueous acidic solution, HA, which dissociates into H^+ and an anion, A^-. In this case, the final current–voltage characteristic is expected to be asymmetric, by a mechanism illustrated in Figure 1. When the anode is on the basic solution side and the cathode is on the acidic solution side (forward bias), the hydrogel will be conductive since the electric field favors entry of both A^- and B^+. The opposite polarity (reverse bias), however, favors removal of A^- and B^+ from the hydrogel and entry of H^+ and OH^-. The latter ions predominantly recombine to form H_2O, however, so the overall concentration of ionic carriers in the hydrogel

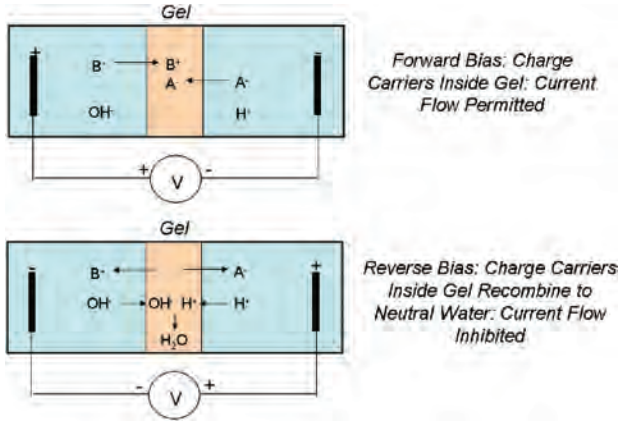

Fig. 1. Operating principle for hydrogel-based electrolytic diode. Acid AH dissociates to H^+ and anion A^-. Base BOH dissociates to OH^- and cation B^+. Top: forward bias. Bottom: reverse bias.

decreases, and so does the conductance. At a high reverse bias, a narrow zone appears in the hydrogel containing almost no ions, and the limiting conductance will be very low. At low positive and negative voltages, diffusive equilibration of A^- and B^+ will also contribute to conductance. The rectification of current predicted by this mechanism resembles that seen in *pn* semiconductor junction diodes, although in the present case there are four mobile charge carriers instead of two.

Previous work on this system involved a poly (vinyl alcohol) (PVA) hydrogel crosslinked with glutaraldehyde.[60–62] The hydrogel was synthesized as a cylinder that was inserted into a narrow, 0.7 mm diameter bore through a polyvinylchloride (PVC) disk of thickness 3.2 mm. This disk separated the two electrolyte chambers. With this system, typically 30–50 min was required for current to reach its stationary value after a change in voltage between chambers. In order to speed up response, we polymerized a hydrogel inside a hard microfabricated structure consisting of a 5×5 array of annular pores (140 μm diameter) etched into a thin (100 μm thick) membrane derived from a silicon wafer. In the center of each pore was a post (40 μm diameter) that was linked to the outer pore wall by miniature silicon tethers, with four tethers on each end of the pore in a "wagon wheel" configuration. Details of fabrication of the tethered microstructure appear elsewhere.[63, 64] A scanning electron micrograph of the structure appears in Figure 2(a).

For the present measurements, a poly(*n*-isopropylacrylamide) (pNIPA) hydrogel crosslinked with *N*,*N*′-methylenebisacrylamide (Bis) was polymerized into the annular gap. The recipe for the hydrogel is given in Table IA. While this hydrogel shrinks at temperatures above 33 °C, it remained completely swollen, filling the gap, throughout the present experiments, which were conducted at room temperature. Figure 2(b) is a micrograph of hydrogels inside the annular micropores.

To measure the current–voltage characteristic, the silicon membrane was bonded with epoxy glue into poly (vinylchloride) (PVC) disk similar to that described previously, with care taken to prevent blockage of the annular micropores. The resulting composite, shown in Figures 2(c, d), was mounted into an electrochemical cell, one chamber (half-cell) containing 0.1 M NH_4OH, and the other containing 0.1 M CH_3COOH. A schematic of the cell is shown in Figure 3. Current (platinum) and voltage (Ag/AgCl) electrodes were introduced into the half-cells, and the solutions filling the chambers were mechanically stirred. Rapid drainage and replenishment of the chamber solutions, and separation of these solutions from the current electrodes by polyurethane foam minimized the accumulation of hydrolysis products. Liquid junction potentials in the voltage-measuring electrodes were suppressed by appropriate salt bridges.[62] Current was controlled by a Keithley 2410 SourceMeter, and voltage across the hydrogel was measured with a high-impedance Keithley 2000 multimeter.

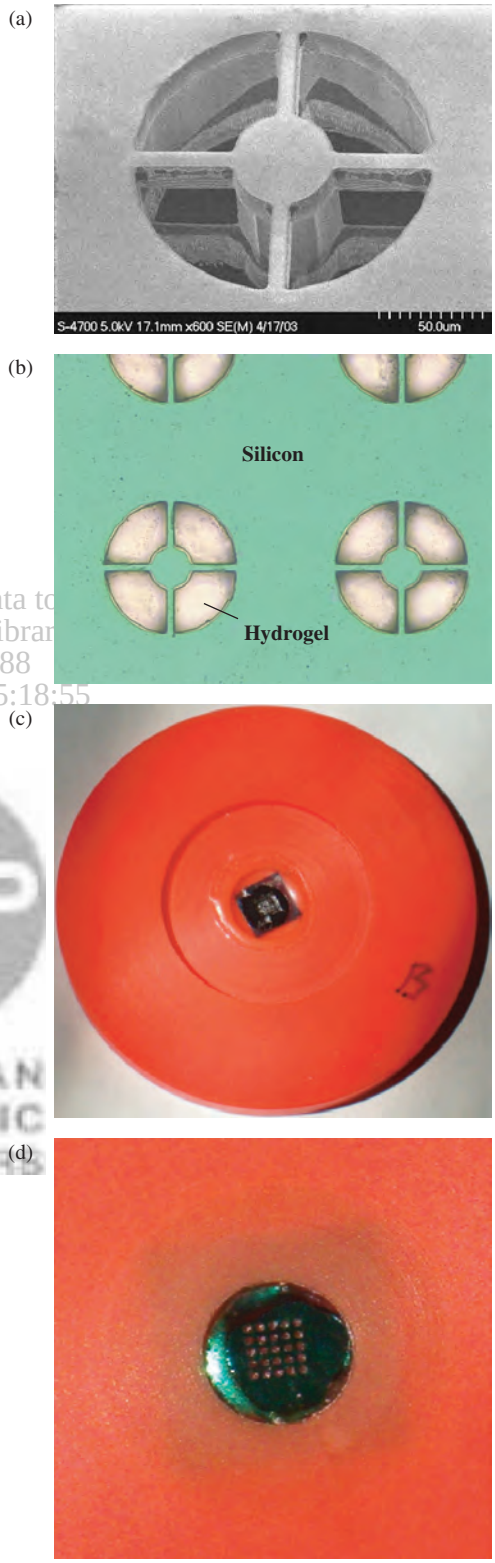

Fig. 2. (a) SEM of annular pore microstructure, with central post suspended by two sets of four tethers connecting it to outer pore wall. (b) Light micrograph of tethered microstructures containing hydrogels. (c) Front view of 5×5 array of tethered microstructures embedded in PVC disk. (d) Rear view, magnified, corresponding to (c). Panels (a) and (b) Reprinted with permission from [63], A. Baldi et al., *Sens. Actuators B* 114, 9 **(2006)**. © 2006, Elsevier.

Table I. Hydrogel recipes. All polymerizations were carried out at room temperature.

A. *p*(NIPA) for microelectrochemical rectifier
Pre-gel solution was composed of 100:1:1000 (w/w/w) *n*-isoproplyacrylamide (NIPA)/methylenebisacrylamide (Bis:crosslinker)/(deionized water). Polymerization was initiated with an (ammonium persulfate)/(*N*,*N*,*N*′,*N*′-tetraethylmethylenediamine) (APS/TEMED:initiator/accelerator) redox couple.

B. *p*(MAA-*co*-AAm) for microcantilever-based pH sensor
Pre-gel solution was composed of 167.5 mg AAm, 50.0 μl MAA, 2.0 μl ethylene glycol dimethacrylate (EGDMA) as crosslinker, 1.1 mg APS, and 25 μl TEMED, all dissolved in 0.7 ml deionized water.

C. *p*(MPBA-*co*-AAm) for microcantilever-based glucose sensor
Pre-gel solution was composed of 52 mg methacrylamidophenyl-boronic acid (MPBA), 0.5 mg Bis, 0.5 mg APS, and 5 μl TEMED, all dissolved in 0.7 ml deionized water.

D. *p*(MAA-*co*-AAm) for pH-sensitive microvalve
Pre-gel solution was composed of 250 mg AAm, 25.0 μl MAA, 1.3 μl EGDMA, 1.1 mg APS, and 13.2 μl TEMED, all dissolved in 0.7 ml deionized water.

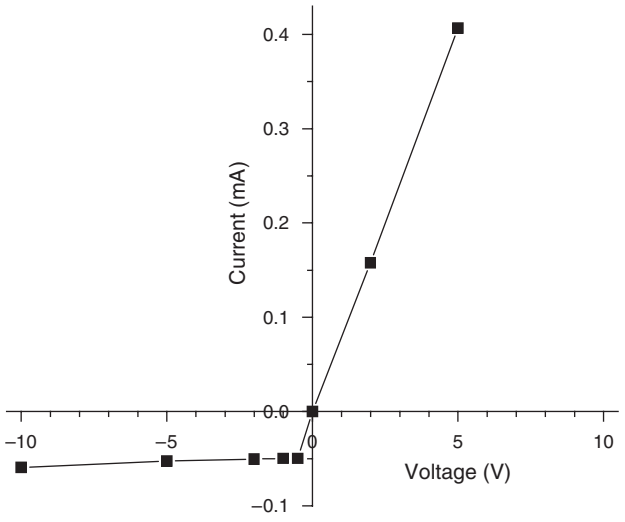

Fig. 4. Example of current–voltage characteristic of array of hydrogels embedded in tethered microstructues (Fig. 2c), as measured in four-electrode electrochemical cell (Fig. 3). Rectification of current due to acid and base in separate adjoining half-cells is demonstrated.

Figure 4 displays a current–voltage characteristic measured with the microstructured silicon-hydrogel composite. As predicted, the characteristic exhibits diode-like rectification. This feature was previously observed with the larger, thicker hydrogels.[62] However, stationarity was achieved within 2–3 min in external conditions in the microstructured systems, much more rapidly than with the previous configuration (∼50 min). We note that the reduction in time-to-steady state would have been reduced even more dramatically if the thickness-squared scaling relation held (see above). Since the silicon membrane was thinner than the PVC disk holder (100 μm versus 3.2 mm), it is conceivable that hydrodynamic and/or chemical diffusion boundary layers may have limited electrodiffusion of electrolytes into and out of the hydrogel (i.e., film control of transport).

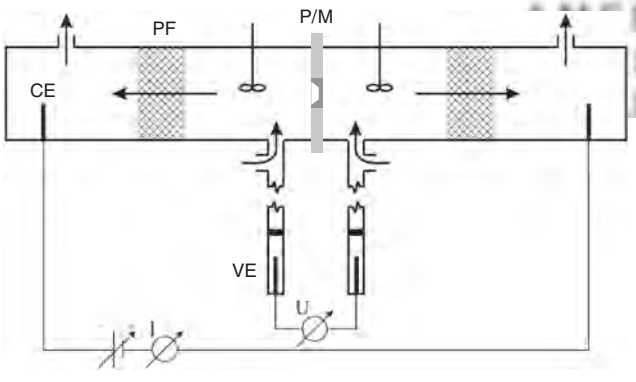

Fig. 3. Four-electrode electrochemical cell used to measure current–voltage characteristic of hydrogels embedded in tethered microstructures, separating solutions of different ionic composition. Solutions flow into half cells, which are magnetically stirred. Solutions exit through compartments containing current electrodes, separated from the half-cells by porous polyurethane foam, which minimizes half-cell solution contamination by electrode hydrolysis products. I—current source; U—voltage meter; CE—current electrode; VE—voltage electrode with salt bridge; P/M—microstructure containing hydrogels, embedded in PVC holder; PF—polyurethane foam. Modified with permission from [62], K. Iván et al., *J. Chem. Phys.* 123, 164510 (**2005**). © 2005, American Institute of Physics.

Small stray currents were detected in controls with no micropores (nonporous silicon membranes of identical thickness to the microporous membranes). These currents were believed to be caused by electrochemical reactions at the silicon/electrolyte interfaces. Attempts to eliminate the stray currents by plasma-enhanced chemical vapor deposition (PECVD) of insulating oxide layers on the membrane surfaces were not completely successful. Since PECVD produces oxide layers with pinhole defects, however, it is not possible to completely dismiss the electrochemical reaction hypothesis. Similarly, a small current drift was detected with prolonged exposure at constant voltage. The stray and drift currents were typically much smaller than the currents reported in Figure 4.

3. MICROCANTILEVER-BASED pH AND GLUCOSE SENSORS

A number of research groups have, in the past several years, described microcantilever-based sensors. For example, bonding of antibodies to microcantilevers permits detection of their respective antigens, either by observing small stress-induced deflection by optical or electrical means, or by monitoring changes in vibration frequency of the microcantilever.[65] Recently, it was shown that by binding a pH-sensitive hydrogel to the top of the microcantilever, deflections could also be detected. Such deflections could be due to changes in mass, or to stresses transferred to the cantilever from the swelling or shrinking hydrogel.[66]

In a previous contribution, we demonstrated a technique for patterning stimuli-sensitive hydrogels on silicon surfaces with resolution down to 2 μm. Unlike other groups

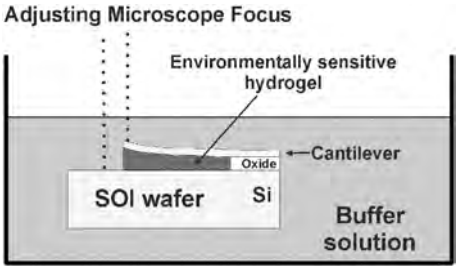

Fig. 5. Schematic of microcantilever with environmentally-sensitive hydrogel underneath.

that have used prepatterning of hydrophilic and hydrophobic surfaces onto the silicon, followed by introduction and polymerization of hydrogel ingredients in aqueous solution, we etched patterns on a continuous layer of dried hydrogel that had been previously synthesized onto a uniformly functionalized silicon surface. In a variation of our technique, we were able to produce patterned hydrogels topped by thin, reflective aluminum surfaces. Changes in hydrogel thickness in response to thermal or chemical changes in the environment could therefore be monitored optically. As will be shown, a similar patterning technique can be used to produce microcantilevers, with the responsive hydrogels located *between* the beams and the silicon substrate, as illustrated in Figure 5. This configuration enables greater force transfer from the hydrogel to the beam, and higher sensitivity.

The microfabrication process is shown in Figure 6. A silicon-on-insulator (SOI) wafer was spin-coated with a layer of photoresist, which was then patterned under a mask (Fig. 6(a)). Deep reactive ion etching (DRIE) was then used to etch the top silicon layer (Fig. 6(b)). Subsequently the buried oxide was removed in a HF/NH_4F buffered oxide etchant for specified times to release the microcantilevers of desired beam overhang length (Fig. 6(c)). The wafer was then cleaned sequentially in acetone, piranha solution, buffered oxide etchant, and deionized water, followed by critical point drying to avoid stiction.

Pre-gel solution was dispensed on top of the device in a vacuum chamber in order to assure complete filling of the pre-gel solution underneath the microcantilevers. The vacuum was subsequently released to push the solution below the cantilevers by air pressure. The pre-gel solution was then clamped between the micromachined wafer and a silanized glass wafer (Fig. 6(d)). After 30 min of polymerization at room temperature, the wafers were separated, with the hydrogel remaining on the silicon wafer. The hydrogel was then dehydrated in acetone and subjected to reactive ion etching (RIE) in an oxygen environment (Fig. 6(e)). During this stage, the patterned microcantilever beams served as a shadow mask, preventing etch of the underlying hydrogel.

Two kinds of hydrogel were loaded into the device: poly(methacrylic acid-*co*-acrylamide) [*p*(MAA-*co*-AAm): for recipe see Table IB], which is pH sensitive, and

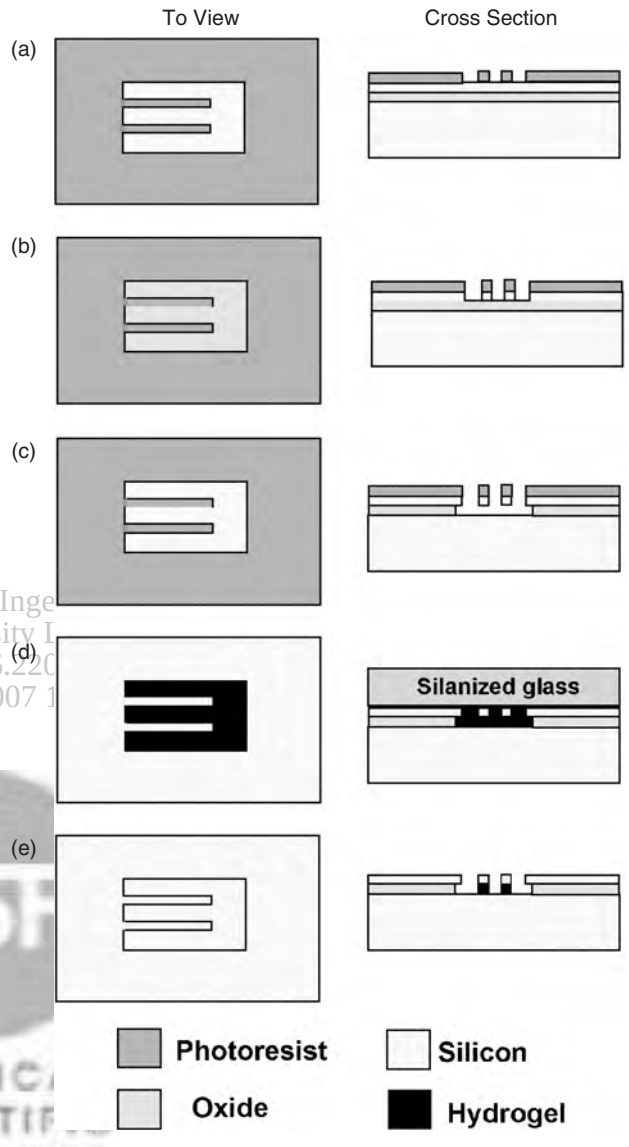

Fig. 6. Microfabrication process for microcantilever/hydrogel. (a) Patterning of photoresist under mask. (b) DRIE etch of top silicon layer. (c) Undercut of top silicon layer by chemical etch of oxide layer, releasing microcantilevers. (d) Loading of pregel solution (under vacuum). Pregel is confined under silanized glass and polymerized. (e) Removal of hydrogel except under microcantilevers by oxygen RIE.

poly(methylacrylamidophenylboronic acid-*co*-acrylamide) [*p*(MPBA-*co*-AAm): for recipe see Table IC], which is both pH and glucose sensitive.

Figure 7 shows SEM images of microcantilever beams with underlying hydrogels in the dehydrated state. The beams were 500 μm long, 20 μm wide, and 2 μm thick. The thickness of the dried hydrogel film was determined to be approximately 1.3 μm by the SEM image.

After fabrication, the device was equilibrated in phosphate buffered saline (PBS) with different pH values and glucose concentrations, and microcantilever deflection was measured using an optical microscope focused on the beam tip, and referenced to the lower, etched surface of the silicon. This optical method had 1 μm resolution.

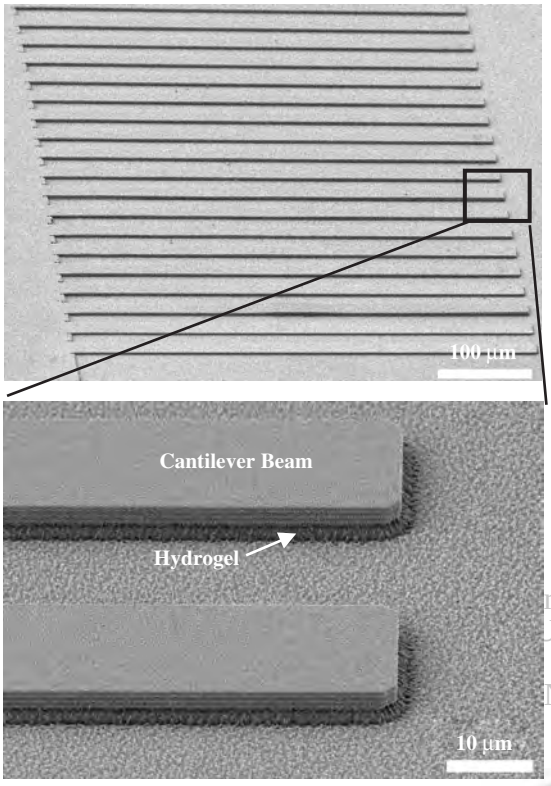

Fig. 7. SEM image of array of microcantilevers. Inset shows dried hydrogel below cantilever beam.

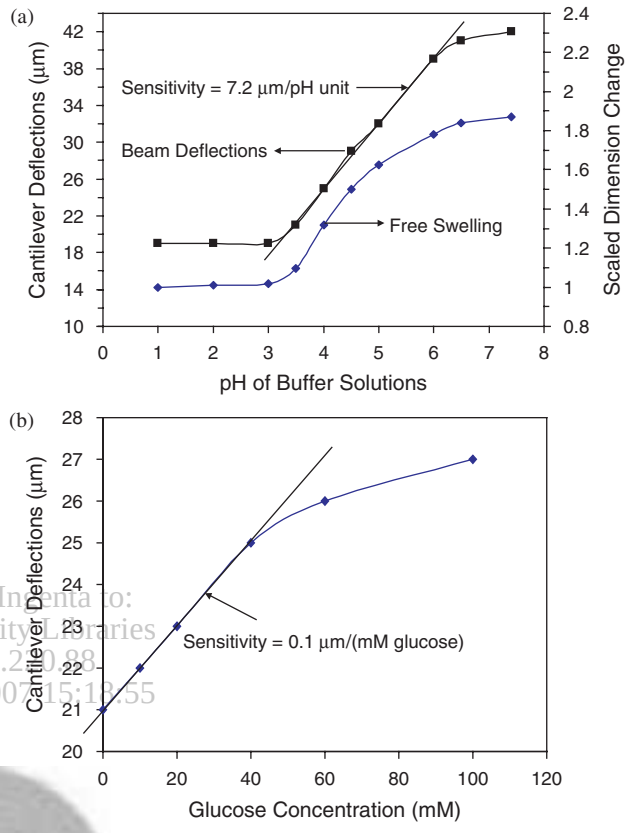

Fig. 8. (a) Effect of pH on microcantilever deflection as a function of pH in PBS solutions at room temperature. Hydrogel is *p*(MAA-*co*-AAm). Also shown is free swelling profile of same hydrogel as function of pH. (b) Effect of glucose concentration on microcantilever deflection in pH 7.4 PBS. Hydrogel is *p*(MPBA-*co*-AAm).

The beams displayed baseline deflection due to the swelling of the dried hydrogel, even before exposure to conditions leading to greater swelling.

Equilibrium deflections of the device with *p*(mAA-*co*-AAm) hydrogel in different pH buffer solutions are shown in Figure 8(a). Stationary displacement of the cantilevers with this hydrogel was achieved within ten seconds upon change of solution pH. The maximum measured deflection was 42 μm at pH 7.4, and the slope of the curve in the linear response range (pH 3.0 to 6.5) was about 7.2 μm/pH unit. This range correlates well with the volume transition range of a free-swelling cylindrical *p*(mAA-*co*-AAm) gel of similar composition, as shown in Figure 8(a).

Figure 8(b) shows the glucose response of the microcantilever over the *p*(MPBA-*co*-AAm) hydrogel, measured at pH 7.4. A slope of about (0.1 μm deflection)/(mM glucose) over the range 0–40 mM was observed. Response to changes in glucose concentration was somewhat more sluggish than for changes in pH (with the different hydrogels), probably because glucose diffuses more slowly than hydrogen ion.

The optical method used was crude in its resolution. Superior (e.g., 1 nm) resolution could be achieved using AFM or laser reflection or interferometric techniques, but these were not explored in the present work. It should be noted that a thousandfold increase in resolution may not be necessary in practice, given the required sensitivities and the presence of "noise" due to interfering analytes.

For the *p*(MPBA-*co*-AAm) hydrogel, interfering species may include small sugars (e.g., fructose, mannose, mannitol), polysaccharides, glycoproteins, and lactate.[28, 67–69] Further, the joint sensitivity of this hydrogel to pH and glucose implies that these signals will interfere with each other. Thus a shift in pH will alter response to glucose. The impact of these interferences on selectivity will depend on the presence and fluctuations in concentrations of the interfering species, along with the relative binding affinities of the various species to the MPBA moiety. Selectivity problems might be mitigated using an array of microcantilevers, with hydrogels exhibiting differing binding and response profiles to the potentially present analytes, and with readout and post-processing of array response. For example, pH-glucose interference might be handled using two microcantilevers, one with *p*(MPBA-*co*-AAm), and the other with *p*(MAA-*co*-AAm).

4. ANALYTE-CONTROLLED MICROVALVE

As indicated previously, researchers have been attempting to exploit stimuli-sensitive hydrogels to control drug release for at least two decades. Major difficulties have arisen due to capacity limitations, size-response tradeoffs,

and mechanical weakness of hydrogels, however. These problems can be circumvented by rendering the hydrogel as a component of an integrated system. For example, rapid gating of flow has been demonstrated in microfluidic networks using micron-dimensioned pH-sensitive hydrogels.[70–73] These hydrogels either swell to fill channels or channel junctions, or shrink away from the channel/junction walls, depending on the pH of the solution flowing through one of the channels impinging on the hydrogel. All channels are in the same plane in these microfluidic systems. In a second example, the tethered microstructures described previously can be filled with temperature-, pH-, or glucose sensitive hydrogels, and shrinkage and reswelling of these hydrogels due to these stimuli can be used to gate fluid flow perpendicular to the plane of the chip containing the microstructures.[63, 64] Both of these structures could be used, in principle, to gate the flow of drug solutions stored in pressurized reservoirs, eliminating the need for a thick hydrogel. In both cases, the hard microstructures provide a substrate against which the hydrogel deforms and exerts its gating action.

Here we describe a microvalve that can gate flow of a drug solution through a microfluidic channel as a result of swelling and deswelling of a hydrogel, which receives its "instructions" by diffusion of an external analyte. We use hydrogen ion (pH change) as a model analyte and *p*(MAA-*co*-AAm) as the hydrogel. The present system is reminiscent of a microvalve that was described previously by our group, but fabrication is simplified.[74] An interesting feature is that both hard and soft materials are used in the mechanical substrate against which the hydrogel swells or shrinks.

As shown in Figure 9(a), the microvalve consists of three layered components. A flexible diaphragm made of polydimethylsiloxane (PDMS, a.k.a. silicone rubber) is clamped between a stiff but porous silicon membrane and a microfluidic channel with inlet and outlet ports. The microchannel and ports are machined into a silicon chip. The top of the diaphragm contains an indentation into which the hydrogel is polymerized. The bottom of the diaphragm has a protrusion, or "boss," that projects into the microchannel. Pores in the top membrane permit diffusion of small solutes and the flow of water into and out of the hydrogel, but the hydrogel is confined between the membrane and the soft silicone diaphragm. Thus any changes in hydrogel swelling due to changes in the external solution are manifested by vertical motion of the diaphragm and boss.

The operating mechanism of the microvalve is illustrated in Figure 9(b). When external solution conditions favor hydrogel swelling, the diaphragm and boss are pushed downwards, closing off the flow inlet. When the hydrogel is caused to shrink by the external stimulus, the diaphragm and boss retract, permitting fluid flow. Note that the swelling of the hydrogel and downward deflection of the diaphragm requires that the swelling pressure of the hydrogel exceeds the overpressure of the fluid in the

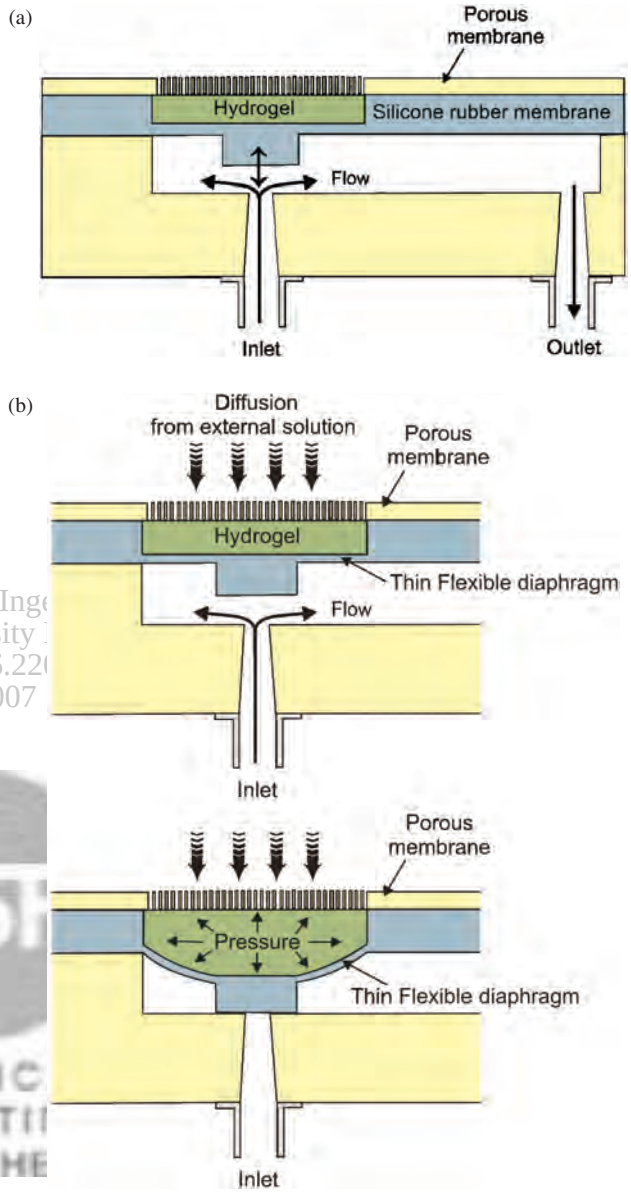

Fig. 9. (a) Schematic of structure of microvalve. (b) Operating principle of microvalve. When external conditions favor unswollen hydrogel, flow channel is open. When hydrogel develops swelling pressure due to external conditions, diaphragm and boss are pushed downward, closing the flow channel.

microchannel. The mechanical stress due to stretching of the diaphragm is negligible.

Figure 10 outlines the fabrication process of the microvalve. A 2 μm thick layer of silicon nitride was deposited on both sides of a silicon wafer. The backside was patterned and KOH etched (450 μm deep) to define the microvalve inlet and outlet (Fig. 10(a)). The top side was patterned (Fig. 10(b)) and DRIE etched to form a 50 μm-deep microchannel connecting the inlet and outlet (Fig. 10(c)). The bottom of the microchannel was then silanized to prevent later stiction with the PDMS boss.

The PDMS diaphragm/boss was fabricated using two molds (Fig. 10(d)). The first mold was a silicon wafer

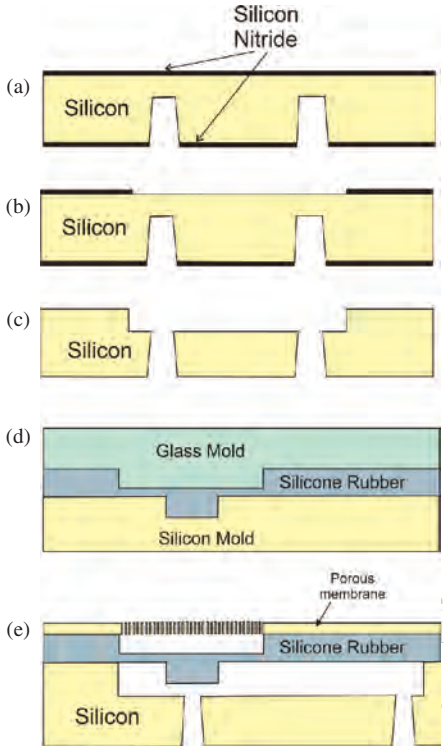

Fig. 10. Construction of microvalve. (a) Deposition of silicon nitride, patterning of backside, and KOH of inlet and outlet ports. (b) Patterning of front side. (c) DRIE etch of front to form microchannel. (d) Casting of PDMS diaphragm/boss between molds. (e) Assembly of microvalve from rigid microporous membrane (top), PDMS diaphragm/boss (middle), and silicon microvalve (bottom).

with a 2 mm × 2 mm × 20 μm DRIE-etched cavity defining the boss. The second mold was a glass slide with a 3 mm × 3 mm × 155 μm projection defining the hydrogel cavity. Both molds were spin-coated with a thin layer of photoresist to assure detachment of the PDMS diaphragm after curing. To cast the diaphragm/boss, a degassed mixture of the two components of a Sylgard™ 184 elastomer kit was introduced between the molds and allowed to cure. The diaphragm/boss was then detached from the molds using acetone.

The rigid porous silicon membrane was fabricated by DRIE etching a 100 μm silicon wafer under a mask consisting of an array of 20 μm holes. A thin layer (0.5 μm) of PECVD oxide was then deposited on both sides of this membrane to render its surface hydrophilic.

The three layers of the microvalve (rigid porous membrane, diaphragm/boss, and microchannel) were assembled with silicone-based adhesive and cured overnight (Fig. 10(e)). The completely assembled device had overall dimensions $10 \times 10 \times 0.75$ mm^3. Microchannel depth was 50 μm and the boss height was 20 μm, leaving a 30 μm gap for fluid flow when the hydrogel was retracted. Figure 11 shows the microchannel etched into the bottom, silicon layer, featuring the inlet and outlet ports.

To load the hydrogel into the microcavity between the porous plate and the diaphragm, pre-gel solution

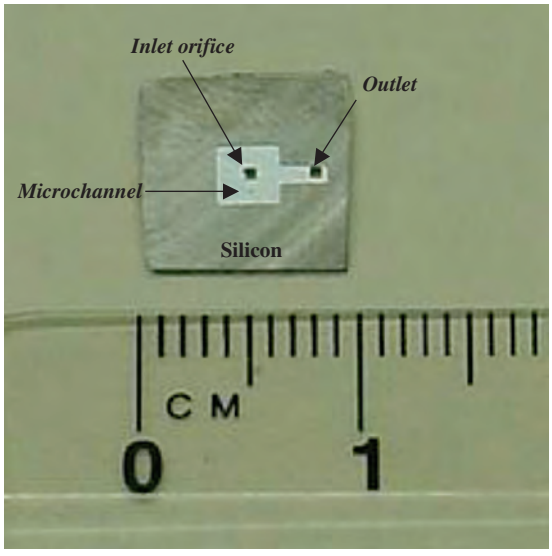

Fig. 11. Silicon microchannel (bottom layer of microvalve), with inlet and outlet ports.

(for recipe see Table ID) was dispensed on top of the porous plate under vacuum. Subsequently, the vacuum was released, and air pressure forced the pre-gel solution into the cavity. Following polymerization, excess hydrogel above the porous plate was stripped off with a razor blade.

The *p*(mAA-*co*-AAm) hydrogel in this device contained a smaller fraction of carboxyl groups (MAA) and cross-linker (EGDMA) than the hydrogel used in the microcantilever studies (Table IB). To study the relative effects of these compositional changes on the hydrogel's swelling, a gel cylinder of the new composition (Table ID) was synthesized inside a glass capillary, and its equilibrium swelling was measured as a function of pH in PBS at room temperature. Results are shown in Figure 12. The linear dimension of the hydrogel in response to pH changes from 3 to 7 increased by 30%, less than the 90% increase in

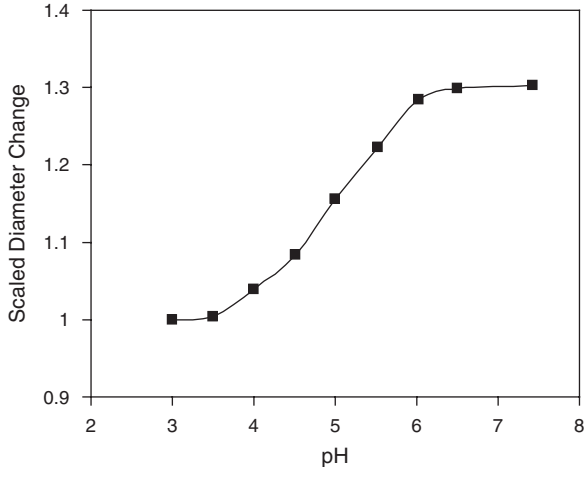

Fig. 12. Free swelling of cylindrical hydrogel as function of pH for *p*(MAA-*co*-AAm) with pre-gel recipe specified in Table ID.

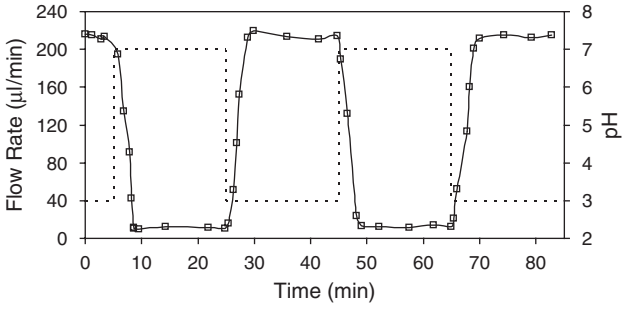

Fig. 13. Flow response of microvalve to alternation of external pH between pH 3.0 and 7.0 in PBS, at room temperature.

the other hydrogel's linear dimension seen under similar conditions (Fig. 8(a)). Since reduced crosslink density should lead to increased swelling, we conclude that the effect of reduced density of ionizable MAA groups was dominant.

To test the pH-sensitive microvalve, the inlet was connected via flexible polyethylene tubing to a column containing distilled water of constant height 60 mm, while the outlet was connected by similar tubing to horizontally-oriented, graduated glass tubing, level with the microvalve. A small port between the polyethylene and glass tubing permitted injection of air bubbles, whose movement was used to determine flow rate. The microvalve was alternately submerged in magnetically-stirred PBS solutions with pH 3.0 (acidic) and 7.0 (neutral), at room temperature.

Figure 13 shows the flow rate of the microvalve in response to pH changes. Flow rates reach steady state within about 3.6 minutes after pH change, and were repeatable within a few μl/min. At pH 3.0, the hydrogel was uncharged and collapsed, so the valve was open. An average flow of about 220 μl/min was observed in this case. At pH 7.4, the hydrogel was swollen, pushing the boss into the inlet. Notice however that the valve did not shut off completely—there was a residual flow of about 10 μl/min. This flow might be attributed either to imperfect closure of the inlet by the boss (i.e. leakage), or to insufficient swelling pressure generated in the hydrogel to clamp the boss completely against the fluid back-pressure. For comparison, the previously constructed microvalve with a solid-state silicon boss shut off flow completely, but was slower to respond than the present design.[74]

While in the present study we focused on pH-sensitivity, a change in hydrogel chemistry could render the microvalve responsive to changes in glucose concentration (using *p*(MPBA-*co*-AAm) hydrogel), temperature (using *p*(NIPA) hydrogel), or concentration of any other analytes that can effect hydrogel swelling. A glucose sensitive microvalve might be considered for closed-loop delivery of insulin in the treatment of Type I diabetes.

In principle, the response time of the valve could be improved by either narrowing the gap between the boss and the inlet valve, or by reducing thickness of the stiff porous membrane and/or hydrogel. In fact, a thinner hydrogel would also require a narrower gap, since the hydrogel's ability to clamp down on the inlet (i.e., its swelling pressure) depends on its swelling ratio. Reduction of thickness of the microporous membrane will ultimately be limited by its ability to withstand hydrogel swelling pressures. It should also be noted that response time may be faster for temperature-sensitive microvalves of similar construction, since heat diffuses faster than molecules, while the slower diffusivity of glucose than for H^+ should lead to slower hydrogel swelling, and hence more sluggish valve response to changes in glucose level.

5. CONCLUSIONS

The three examples presented here demonstrate that hydrogels can be embedding within microstructures, and that hydrogel function can be improved by such immobilization. The microstructures contain hard (silicon) and/or soft (PDMS) elements. Advantages of embedding include
(1) the hydrogel can be placed permanently in a definite location where it can perform its task repeatedly,
(2) hydrogel mechanical failure may become less of an issue when the primary action is swelling against a well-defined structure, and
(3) reduced size leads to faster mass transfer and chemo-mechanical response.

While we were able to show relatively rapid response in all three systems studied, it should be noted that with the small device and hydrogel dimensions, response rates could be limited by external fluid and mass transfer boundary layers. Further acceleration of response might be achieved by more vigorous agitation or stirring of the external environment, when possible.

Response specificity may be an issue, since individual hydrogels can respond to multiple stimuli. The small size of the considered systems suggests that this problem might be approached by array techniques. In some cases, improved specificity might be engineered into the system by chemical redesign of the hydrogels' responsive elements.[75]

Acknowledgments: This work was supported in part by NIH grant EB003125. We thank Drs. Antonio Baldi and Yuandong Gu for early discussion of the tethered microstructures.

References and Notes

1. A. J. Grodzinsky, *CRC Crit. Rev. Biomed. Eng.* 9, 133 (**1985**).
2. D. Narmoneva, J. Wang, and L. Setton, *Biophys. J.* 81, 3066 (**2001**).
3. F. Horkay, I. Horkayne-Szakaly, and P. Basser, *Biomacromolecules* 6, 988 (**2005**).
4. B. D. Ratner, Biocompatibility of Clinical Implant Materials, edited by D. F. Williams, CRC Press, Boca Raton (**1981**), Vol. 2, p. 145.
5. M. F. Refojo and F.-L. Leong, *J. Memb. Sci.* 4, 415 (**1979**).

6. F. Helfferich, Ion Exchange, Dover, Toronto (**1995**).
7. S. H. Gehrke, G. Agrawal, and M.-C. Yang, in Polyelectrolyte gels. *ACS Symp. Ser.*, edited by R. S. Harland and R. K. Prud'homme, American Chemical Society, Washington, DC (**1992**), Vol. 480, p. 211.
8. J. Kobayashi, A. Kikuchi, K. Sakai, and T. Okano, *J. Chromatogr. A* 958, 109 (**2002**).
9. E. Kokufuta, *Prog. Polym. Sci.* 17, 647 (**1992**).
10. N. A. Peppas, Hydrogels in Medicine and Pharmacy, CRC Press, Boca Raton, FL (**1986**).
11. Y. Hirokawa and T. Tanaka, *J. Chem. Phys.* 81, 6379 (**1984**).
12. S. Sasaki, H. Kawasaki, and H. Maeda, *Macromolecules* 30, 1847 (**1997**).
13. R. Yoshida, K. Uchida, Y. Kaneko, K. Sakai, A. Kikuchi, Y. Sakurai, and T. Okano, *Nature* 374, 240 (**1995**).
14. J. Ricka and T. Tanaka, *Macromolecules* 17, 2916 (**1984**).
15. R. A. Siegel and B. A. Firestone, *Macromolecules* 21, 3254 (**1988**).
16. L.-C. Dong and A. S. Hoffman, *J. Control. Rel.* 13, 21 (**1990**).
17. S. H. Gehrke and E. L. Cussler, *Chem. Eng. Sci.* 44, 559 (**1989**).
18. H. Kawasaki, S. Sasaki, and H. Maeda, *J. Phys. Chem. B.* 101, 5089 (**1997**).
19. S. Kazakov, M. Kaholek, D. Kudasheva, I. Teraoka, M. K. Cowman, and K. Levon, *Langmuir* 19, 8086 (**2003**).
20. I. Ohmine and T. Tanaka, *J. Chem. Phys.* 77, 5725 (**1982**).
21. B. A. Firestone and R. A. Siegel, *J. Biomater. Sci. Polym. Ed.* 5, 433 (**1994**).
22. T. Tanaka, I. Nishio, S. T. Sun, and S. Ueno-Nisho, *Science* 218, 467 (**1982**).
23. S. R. Eisenberg and A. J. Grodzinsky, *J. Memb. Sci.* 19, 173 (**1984**).
24. M. Zrinyi, L. Barsi, D. Szabo, and H. G. Kilian, *J. Chem. Phys.* 106, 5685 (**1997**).
25. M. Irie, *Pure and Appl. Chem.* 62, 1495 (**1990**).
26. A. Suzuki and T. Tanaka, *Nature* 346, 345 (**1990**).
27. D. Shiino, A. Kubo, Y. Murata, Y. Koyama, K. Kataoka, A. Kikuchi, Y. Sakurai, and T. Okano, *J. Biomater. Sci. Polym. Ed.* 7, 697 (**1996**).
28. V. L. Alexeev, A. C. Sharma, A. V. Goponenko, S. Das, I. K. Lebedev, C. S. Wilcox, D. N. Finegold, and S. A. Asher, *Anal. Chem.* 75, 2316 (**2003**).
29. M. Shibayama, M. Uesaka, S. Inamoto, H. Mihara, and S. Nomura, *Macromolecules* 29, 885 (**1996**).
30. T. Miyata, N. Asami, and T. Uragami, *Nature* 399, 766 (**1999**).
31. T. Tanaka, *Phys. Rev. Lett.* 40, 820 (**1978**).
32. Y. Li and T. Tanaka, *Annu. Rev. Mater. Sci.* 22, 243 (**1992**).
33. Y. Osada and J. P. Gong, *Prog. Polym. Sci.* 18, 187 (**1993**).
34. P. G. de Gennes, K. Okamura, M. Shahinpoor, and K. J. Kim, *Europhys. Lett.* 50, 513 (**2000**).
35. I. S. Han, M. H. Han, J. Kim, S. Lew, Y. J. Lee, F. Horkay, and J. Magda, *Biomacromolecules* 3, 1271 (**2002**).
36. K. Ishihara, M. Kobayashi, N. Ishmaru, and I. Shinohara, *Polymer J.* 16, 625 (**1984**).
37. G. Albin, T. A. Horbett, and B. D. Ratner, *J. Control. Rel.* 2, 153 (**1985**).
38. R. A. Siegel, M. Falamarzian, B. A. Firestone, and B. C. Moxley, *J. Control. Rel.* 8, 179 (**1988**).
39. Y. H. Bae, T. Okano, R. Hsu, and S. W. Kim, *Makromol. Chem. Rapid. Commun.* 8, 481 (**1987**).
40. R. Yoshida, K. Sakai, T. Okano, and Y. Sakurai, *J. Biomater. Sci. Polym. Ed.* 3, 243 (**1992**).
41. K. Kataoka, H. Miyazaki, M. Bunya, T. Okano, and Y. Sakurai, *J. Am. Chem. Soc.* 120, 12694 (**1998**).
42. N. Peppas and W. Leobandung, *J. Bomater. Sci. Polym. Ed.* 15, 124 (**2004**).
43. J. Kopecek, *Eur. J. Pharmaceut.* 20, 1 (**2003**).
44. A. S. Hoffman, *Pure and Appl. Chem.* 56, 1329 (**1984**).
45. S. H. Gehrke, G. P. Andrews, and E. L. Cussler, *Chem. Eng. Sci.* 41, 2153 (**1986**).
46. Y. Tanaka, J. P. Gong, and Y. Osada, *Prog. Polym. Sci.* 30, 1 (**2005**).
47. J. P. Gong, Y. Katsuyama, T. Kurokawa, and Y. Osada, *Adv. Mater.* 15, 1155 (**2003**).
48. K. Haraguchi and T. Takehisa, *Adv. Mater.* 14, 1120 (**2002**).
49. Y. Okamura and K. Ito, *Adv. Mater.* 13, 485 (**2001**).
50. T. Tanaka and D. Fillmore, *J. Chem. Phys.* 70, 1214 (**1979**).
51. P. E. Grimshaw, J. H. Nussbaum, A. J. Grodzinsky, and D. M. Yarmush, *J. Chem. Phys.* 93, 4462 (**1990**).
52. T. Tomari and M. Doi, *J. Phys. Soc. Jpn.* 63, 2093 (**1994**).
53. J. Crank, The Mathematics of Diffusion, 2nd edn., Oxford University Press, Oxford (**1975**).
54. H. Yasuda, C. E. Lamaze, and A. Peterlin, *J. Polym. Sci. Pt. A-2* 9, 1117 (**1971**).
55. L. Johansson and J. E. Lofroth, *Macromolecules* 24, 6024 (**1991**).
56. L. Masaro and X. X. Zhu, *Prog. Polym. Sci.* 24, 731 (**1999**).
57. B. Amsden, *Macromolecules* 34, 1430 (**2001**).
58. Z. B. Hu, C. G. Wang, K. D. Nelson, and R. C. Eberhart, *ASAIO J.* 46, 431 (**2000**).
59. M. J. Serpe, K. A. Yarmey, C. M. Nolan, and L. A. Lyon, *Biomacromolecules* 6, 408 (**2005**).
60. K. Iván, M. Wittman, P. Simon, Z. Noszticzius, and J. Vollmer, *Phys. Rev. E* 70, 061402 (**2004**).
61. K. Iván, P. Simon, M. Wittman, and Z. Noszticzius, *J. Chem. Phys.* 123, 164509 (**2005**).
62. K. Iván, M. Wittman, P. Simon, Z. Noszticzius, and D. Snita, *J. Chem. Phys.* 123, 164510 (**2005**).
63. A. Baldi, M. Lei, Y. Gu, R. A. Siegel, and B. Ziaie, *Sens. Actuators B* 114, 9 (**2006**).
64. B. Ziaie, A. Baldi, M. Lei, Y. Gu, and R. A. Siegel, *Adv. Drug Deliv. Revs.* 56, 145 (**2004**).
65. K. M. Hansen and T. Thundat, *Methods* 37, 57 (**2005**).
66. J. Z. Hilt, A. K. Gupta, R. Bashir, and N. A. Peppas, *Biomed. Microdev.* 5, 177 (**2003**).
67. M. Lei, A. Baldi, E. Nuxoll, R. A. Siegel, and B. Ziaie, *Diabet. Technol. Therap.* 8, 112 (**2006**).
68. J. P. Lorand and J. O. Edwards, *J. Org. Chem.* 24, 709 (**1959**).
69. S. Kabilan, A. J. Marshall, F. K. Sartain, M.-C. Lee, H. A. X. Yang, J. Blyth, N. Karangu, K. James, J. Zeng, D. Smith, A. Domschke, and C. R. Lowe, *Biosens. Bioelectron.* 20, 1602 (**2005**).
70. K.-F. Arndt, D. Kuckling, and A. Richter, *Polym. Adv. Technol.* 11, 496 (**2000**).
71. D. J. Beebe, *Nature* 404, 588 (**2000**).
72. M. E. Harmon, M. Tang, and C. W. Frank, *Polymer* 44, 4547 (**2003**).
73. D. Kuckling, J. Hoffman, M. Plotner, D. Ferse, K. Kretschmer, H.-J. P. Adler, K.-F. Arndt, and R. Reichelt, *Polymer* 44, 4455 (**2003**).
74. A. Baldi, Y. Gu, P. Loftness, R. A. Siegel, and B. Ziaie, *IEEE J. Microelectromech. Syst.* 12, 613 (**2003**).
75. V. Alexeev, S. Das, D. N. Finegold, and S. A. Asher, *Clinical Chemistry* 50, 1 (**2004**).

Received: 5 December 2005. Accepted: 17 April 2006.